WILEY InterScience® DISCOVER SOMETHING GREAT

PROTEINS STRUCTURE ■ FUNCTION ■ BIOINFORMATICS

Electrostatic contribution to the thermodynamic and kinetic stability of the homotrimeric coiled coil Lpp-56: A computational study

Saša Bjelić,[1] Silke Wieninger,[2,3] Ilian Jelesarov,[1] and Andrey Karshikoff[2]*

[1] Biochemisches Institut der Universität Zürich, Winterthurerstr, Zürich, Switzerland

[2] Department of Biosciences and Nutrition, Karolinska Institute, Stockholm, Sweden

[3] ERASMUS programme student on leave from University of Bayreuth

ABSTRACT

The protein moiety of the Braun's* E. coli *outer membrane lipoprotein (Lpp-56) is an attractive object of biophysical investigation in several aspects. It is a homotrimeric, parallel coiled coil, a class of coiled coils whose stability and folding have been studied only occasionally. Lpp-56 possesses unique structural properties and exhibits extremely low rates of folding and unfolding. It is natural to ask how the specificity of the structure determines the extraordinary physical chemical properties of this protein. Recently, a seemingly controversial data on the stability and unfolding rate of Lpp-56 have been published (Dragan* et al.*, Biochemistry 2004;43: 14891–14900; Bjelic* et al.*, Biochemistry 2006;45:8931–8939). The unfolding rate constant measured using GdmCl as the denaturing agent, though extremely low, was substantially higher than that obtained on the basis of thermal unfolding. If this large difference arises from the effect of screening of electrostatic interactions induced by GdmCl, electrostatic interactions would appear to be an important factor determining the unusual properties of Lpp-56. We present here a computational analysis of the electrostatic properties of Lpp-56 combining molecular dynamics simulations and continuum* pK *calculations. The pH-dependence of the unfolding free energy is predicted in good agreement with the experimental data: the change in* ΔG *between pH 3 and pH 7 is* $\sim$*60 kJ mol*$^{-1}$*. The results suggest that the difference in the stability of the protein observed using different experimental methods is mainly because of the effect of the reduction of electrostatic interactions when the salt (GdmCl) concentration increases. We also find that the occupancy of the interhelical salt bridges is unusually high. We hypothesize that electrostatic interactions, and the interhelical salt bridges in particular, are an important factor determining the low unfolding rate of Lpp-56.

Proteins 2008; 70:810–822.

Key words: electrostatic interactions; protein stability; unfolding kinetics; molecular dynamics; salt bridge; coiled coil.

INTRODUCTION

The coiled coil is a ubiquitously encountered structural motif in proteins.[1] Amino acid stretches bearing direct repetition of the *abcdef* heptad pattern form two-, three-, or higher-order superhelices. The strandedness (degree of oligomerisation), the orientation (parallel vs. antiparallel), and the registry (in-register vs. out-of-register) are dictated by the nature of mostly aliphatic side chains occupying positions *a* and *d*, in an intimate interplay with the nature of mostly charged side chains occupying positions *e* and *g*. Given the apparent simplicity of the motif, coiled coils have attracted attention as a model for investigating the sequence–structure–energy relationships in protein folding. However, the main body of knowledge about coiled coil folding stems from investigations of short, dimeric, three- to five-heptad long species. Higher-order coiled coils are less well characterized.

The 56 amino acid long protein moiety of the *E. coli* outer membrane protein (henceforth referred to as Lpp-56) is a parallel, in-register, trimeric coiled coil.[2] The physiological importance of this protein in maintaining the structural integrity of the *E. coli* cell wall has been reviewed.[3] Recently, we have determined the equilibrium stability and the rates of unfolding and refolding of Lpp-56 at pH 7.[4] In this study we used GdmCl to shift the equilibrium between folded trimer and unfolded monomer, and to modulate the refolding and unfolding rates. The unfolding free energy, ΔG^{Gdm}, obtained by extrapolation to zero denaturant according to the linear extrapolation method is 79 $\pm$ 10 kJ mol^{-1}. A substantially larger value, $\Delta G^{\mathrm{therm}}$ = 137 kJ mol^{-1}, has been determined

Grant sponsor: Swiss National Science Foundation; Grant number: 3100A0-100197.
*Correspondence to: Andrey Karshikoff, Ph.D., Dr.Sci., Karolinska Institutet, Dep. Biosciences and Nutrition, S-14157 Huddinge, Sweden. E-mail: aka@csb.ki.se
Received 17 January 2007; Revised 20 March 2007; Accepted 13 April 2007
Published online 29 August 2007 in Wiley InterScience (www.interscience.wiley.com). DOI: 10.1002/prot.21585

from calorimetric experiments.[5] Interestingly, ΔG^{therm} at pH 3, where salt bridges are believed to be disrupted by protonation of acidic side chains, is on the order of 70 kJ mol^{-1}.[5] Since GdmCl is a salt it is intuitive to assume that the discrepancy can be attributed to screening of electrostatic interactions when the unfolding free energy is evaluated by linear extrapolation of data collected at high salt (GdmCl) conditions, leading to a severe underestimation of ΔG^{Gdm}. However, we reasoned[4] that if Lpp-56 obeys the two-state unfolding model (neither we, nor Dragan *et al.* have detected intermediate states) the contribution of electrostatic interactions that are eliminated by salt should be between 10 and 20 kJ mol^{-1}. The latter value is pretty close to previous estimates[6–11] of the magnitude of the electrostatic contribution to protein stability, but is rather low to explain the difference in the unfolding free energy obtained by us and by Dragan *et al.*

One striking property of Lpp-56 is its extremely low unfolding rate. Our own estimate[4] of the unfolding rate constant is on the order of 10^{-10} to 10^{-13} s^{-1}. The data of Dragan *et al.*[5] predict an even lower unfolding rate constant, on the order of 10^{-21} s^{-1}. Both estimates demonstrate an extremely high kinetic stability of Lpp-56, yet the difference appears too large to be explained by the charge screening effect of GdmCl used in our experiments. Nevertheless, based on the steep dependence of the activation unfolding energy on GdmCl concentration at pH 7 and the much faster unfolding at pH 3, we speculated that there is a large electrostatic contribution to the free energy barrier for unfolding.

Indeed, each Lpp-56 polypeptide contains eight acidic side chains (exclusively aspartic acid) and eight basic side chains (four lysines and four arginines). In addition, the C-terminal carboxylates and the three tyrosines (one per chain) are potentially capable to participate in salt bridge formation. As in other coiled coils, reflecting the repetitive heptad organization of the molecule, the interhelical salt bridges form a system of rings girdling the three-helix bundle of Lpp-56 along its length (see Fig. 1).

These peculiarities of Lpp-56, together with the large number of potential salt bridges seen in the crystal structure[2] motivated us to investigate the role of electrostatic interactions in the stabilization of the native structure of Lpp-56. To our knowledge, there are no published experimental data on ionization constants of the titratable groups or a potentiometric titration curve of Lpp-56, which can facilitate the analysis of electrostatic interactions. Therefore, our investigation essentially relies on theoretical prediction of ionization equilibria. This creates some difficulties in the quantitative assessment of the results, especially results concerning the thermodynamic stability of the protein. In spite of this, we extract information about the magnitude of the screening effect of salt on electrostatic interactions. Furthermore, we demonstrate the presence of unusually stable salt bridges and formulate a hypothesis explaining the extremely low unfolding rate of Lpp-56.

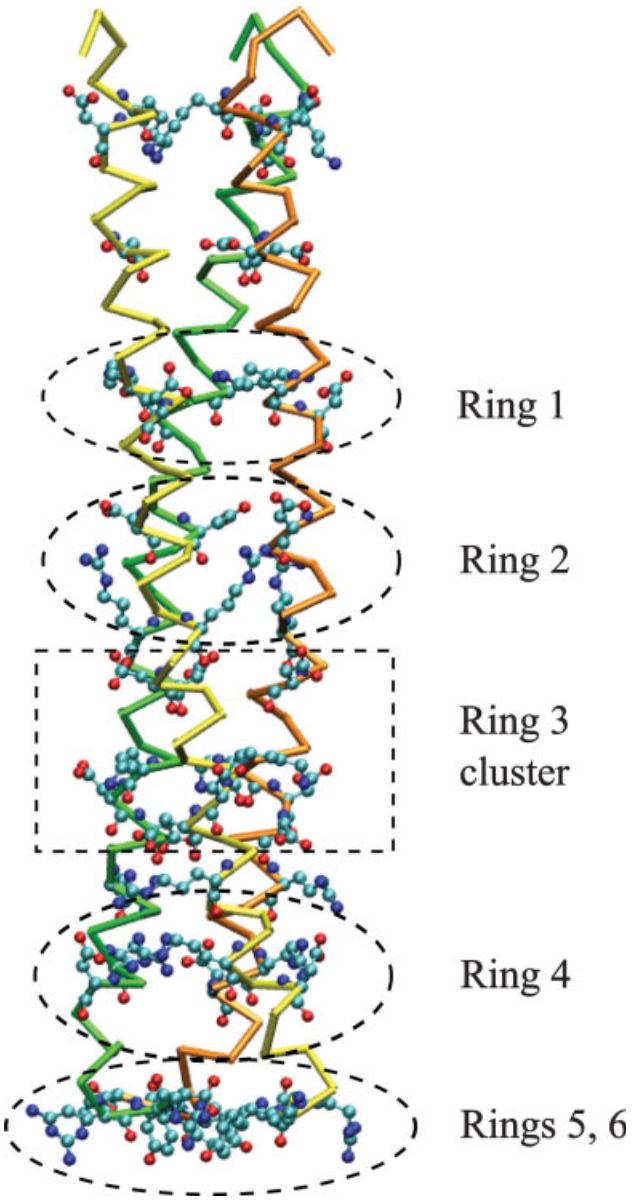

Figure 1

Titratable side chains in Lpp-56. The groups forming salt bridges are grouped in rings along the rod-like molecule (see also Table III). The description of the rings is given in some detail in section "Role of the salt bridges in unfolding kinetic of Lpp-56." In the shown orientation the N-terminus is on top. Image reproduced by the VMD software.[12]

COMPUTATIONAL METHOD

Theoretical background

Our approach basically does not differ from that of Yang and Honig.[13] Here we present the differences in

the strategy chosen for the calculations. The electrostatic term of the free energy of unfolding at given pH can then be obtained (see Yang and Honig[13] and the references therein) by

$$\Delta G^{\mathrm{el}}(\mathrm{pH}) = \Delta G^{\mathrm{el,U}}(\mathrm{pH}) - \Delta G^{\mathrm{el,F}}(\mathrm{pH})$$

$$= 2.3RT \int_{\mathrm{pH}_0}^{\mathrm{pH}} \left(\nu^{\mathrm{U}}(\mathrm{pH}) - \nu^{\mathrm{F}}(\mathrm{pH})\right) \mathrm{dpH}, \qquad (1)$$

where

$$\nu^{\mathrm{U,F}}(\mathrm{pH}) = \sum_{i=1}^{N} \theta_i^{\mathrm{U,F}}(\mathrm{pH}) \qquad (2)$$

are the average number of protons bound to the protein molecule in the unfolded (U) and in the folded (F) state, respectively, θ_ι is the degree of protonation of titratable site i, and N is the total number of titratable sites. $\Delta G^{\mathrm{el,U}}$ and $\Delta G^{\mathrm{el,F}}$ are the electrostatic free energies of the unfolded and folded states, respectively, and are defined in respect to a certain reference state. Different reference states can be chosen. For instance, Yang and Honig[13] have chosen pH equal to 0, whereas Langella *et al.*[14] defined it as an abstract state, at which all titratable groups in the protein are in their neutral forms. In this work, we choose another abstract reference state; that is an extreme acidic pH, pH_0, at which the protein is fully protonated in both, the folded and unfolded states. Obviously, $\theta_\iota^{\mathrm{U}}(\mathrm{pH}_0) = \theta_\iota^{\mathrm{F}}(\mathrm{pH}_0)$. Following Bashford and Karplus[15,16] the degree of protonation of site i is given by:

$$\theta_i(\mathrm{pH}) = \frac{\sum_{\{\mathbf{x}\}} x_i e^{-E(\mathbf{x},\mathrm{pH})/RT}}{\sum_{\{\mathbf{x}\}} e^{-E(\mathbf{x},\mathrm{pH})/RT}}. \qquad (3)$$

The energy $E(\mathbf{x},\mathrm{pH})$ is the electrostatic energy corresponding to a single protonation state, $\mathbf{x}$, of the protein molecule:

$$E(\mathbf{x},\mathrm{pH}) = 2.3RT \sum_{i}^{N} x_i(\mathrm{p}K_{i,\mathrm{int}} - \mathrm{pH}) + \frac{1}{2}\sum_{\substack{i,j \\ i\neq j}} W_{ix_i,jx_j}. \qquad (4)$$

A single protonation state is determined by the sequence $\mathbf{x} = (x_1,x_2,\ldots, x_i,x_j,\ldots, x_N)$, the elements of which describe the microscopic protonation states of the individual titratable sites. In this work, we assume that the individual titratable sites have only two microscopic states: $x_i = 0$ (protonated) and $x_i = 1$ (deprotonated). The electrostatic energy of interaction between sites i and j in protonation state x_i and x_j, respectively, is given by W_{ix_i,jx_j}, whereas $\mathrm{p}K_{i\mathrm{int}}$ is the intrinsic pK value of site i defined as

$$\mathrm{p}K_{\mathrm{int}} = \mathrm{p}K_{i,\mathrm{mod}} + \Delta\mathrm{p}K_{i,\mathrm{Born}} + \Delta\mathrm{p}K_{i,\mathrm{pc}}. \qquad (5)$$

The first term in the right hand side of the above equation, $\mathrm{p}K_{i,\mathrm{mod}}$, is the equilibrium constant of a model compound (Table I). The correction $\Delta\mathrm{p}K_{i,\mathrm{Born}}$ accounts for the desolvation of site i, whereas $\Delta\mathrm{p}K_{i,\mathrm{pc}}$ is the pK shift caused by the electrostatic interactions of this site with the partial atomic charges of the protein molecule that do not belong to any titratable group.

Equations (3) and (4) are valid for both folded and unfolded states. The calculations, however, are based on different models. In the case of folded proteins the values of W_{ix_i,jx_j}, $\Delta\mathrm{p}K_{i,\mathrm{Born}}$ and $\Delta\mathrm{p}K_{i,\mathrm{pc}}$ are calculated on the basis of the three-dimensional structure of the protein. Prediction of the electrostatic properties of proteins based on crystal structures often faces difficulties arising from the fixed three-dimensional structure itself. For instance, due to the effect of the crystal contacts, regions of the protein molecule may preferably adopt conformations that are not populated in solution. In general, the X-ray structure does not necessarily represent the ensemble of structures of the protein in solution. This property of the protein structure, which we refer to as conformational flexibility, is one of the sources of discrepancy between prediction and experiment. Variety of methods exist that account in different extent for the conformational flexibility.[13,19–25]

Table I
Values of $\mathrm{p}K_{mod}$ and pK of Lpp-56 Calculated for I = 0.12

Group	$\mathrm{p}K_{\mathrm{mod}}$[a]	*A*	*B*	*C*
N-term	8.2[b]	8.0	7.2	8.0
Asp07	4.0	2.0	2.8	1.9
Asp12		3.5	3.4	3.5
Asp21		3.3	3.2	3.2
Asp26		−1.9	−4.8	−3.7
Asp33		0.8	1.8	1.5
Asp39		2.6	3.5	0.2
Asp40		2.4	1.8	3.8
Asp49		2.5	2.6	0.8
Tyr55	9.4	16.1	15.9	16.0
Lys05	10.4	10.3	10.3	10.1
Lys19		10.6	10.2	10.7
Lys38		13.9	13.1	13.1
Lys54		13.0	12.8	13.2
Arg31	12.0	16.6	13.9	16.2
Arg43		14.4	12.9	14.0
Arg47		13.9	16.5	14.1
Arg56		12.5	12.6	12.5
C-ter	3.6[c]	−3.8	−2.9	−3.0

The individual helices are designated by *A*, *B*, and *C*.
[a]Values taken from Refs. 16, 17.
[b]pK of glycine amide (science.smith.edu/departments/Biochem/Biochem_353/Common_Buffers.htm).
[c]pK of *N*-acetyl glycine.[18]

DOI 10.1002/prot

The combination of molecular dynamics (MD) and pK calculations is an alternative approach.[13,26–30] The combination of MD and pK calculations results in an overall improvement of the theoretically predicted pK values. However, discrepancies between experimental and calculated pK values often remain for groups buried in the protein interior. Among different reasons one can mention the limited simulation time, as well as the bias of the simulation by the choice of the protonation state of the protein. Nevertheless, in our opinion, this method is currently the most promising one. In the investigation presented in this article, the ionization equilibria in the folded state of Lpp-56 have been calculated by a continuum electrostatic model combined with MD simulation as described in our previous work.[31]

The titration curves of unfolded proteins, $\nu^{U}(\mathrm{pH})$, are often calculated on the basis of the standard ionisation constants of the different types of titratable groups. In this null approximation electrostatic interactions are in fact ignored. This approximation is insufficient for prediction of quantities, such as the electrostatic term of unfolding energy.[32] The models of denatured state of proteins use different approximation mainly reflecting the increased hydration of the titratable groups.[33–36] A more general model of denatured state has been proposed by Zhou.[37–40] In this model, the denatured protein molecule is treated as a Gaussian chain immersed in a dielectric medium for which electrostatic interactions are calculated by means of the Debye-Hückel theory. Recently, we have proposed an approach[41–43] which is based on the continuum dielectric model and is ideologically very close to that of Zhou. In our model, the unfolded protein molecule is represented as a material with low dielectric constant, ε_p between 20 and 40, immersed in the high permittivity medium of the solvent, $\varepsilon_s > \varepsilon_p$. The shape of the dielectric cavity can be considered as an average over all possible conformations of the polypeptide chain, which results in a sphere inside which most of the protein atoms reside.[41] At equilibrium, the titratable groups are approximated as charge points allocated on the surface of the sphere. The charge distributions corresponding to the variety of conformers which an unfolded protein can adopt is reflected by the different configurations of a virtual chain connecting consecutively the charges on the surface of the dielectric cavity.[41] The model has been successfully applied for calculation of the pH-dependence of the unfolding free energy of several proteins.[44] This model has been employed in the presented study.

Molecular dynamics simulation

The X-ray structures of Lpp-56 (PDB entry 1eq7) and GCN4 leucine zipper (PDB entry 2zta) were used as starting point for MD simulations. The simulations were carried out with the OPLS all-atom force field, as implemented in the GROMACS simulation suite (version 3.3.1).[45] The structure was solvated with TIP4 water[46] at ~150 mM NaCl (plus additional ions to neutralize the total system). In the cubic periodic box the minimum distance between the protein and the end of the box was more 1.5 nm. After minimization using Steepest Descent model with a tolerance of 1000 kJ mol^{-1} nm^{-1}, the system was simulated for 400 ps with harmonic position restrain on all Cα-atoms (force constant: 1000 kJ mol^{-1} nm^{-2} and additional 100 ps with a force constant of 100 kJ mol^{-1} nm^{-2}) in order to allow relaxation of the solvent molecules. LINCS[47] and SETTLE[48] algorithms were applied. The integration step was 2 fs. Short-range electrostatics were calculated explicitly, and long range electrostatic interactions were calculated using the particle-mesh Ewald method.[49] Lennard-Jones interactions were cut at a distance of 1 nm, a long-range correction for the energy and the pressure was applied. The system was coupled to Berendsen temperature bath separately for the protein and the solvent ($\tau_t = 0.1$ ps) and to a Berendsen pressure bath ($\tau_p = 0.1$ ps).[50] Trajectory visualization and analyzing were made in part using VMD.[12]

pK calculations

The computational approach used to calculate $\theta_i^{F}(\mathrm{pH})$, and respectively $\nu^{F}(\mathrm{pH}_0)$, has been described earlier.[31,51] The values of $\mathrm{p}K_{\mathrm{mod}}$ are listed in Table I. The values of $\Delta\mathrm{p}K_{i,\mathrm{Born}}$ and $\Delta\mathrm{p}K_{i,\mathrm{pc}}$, required to complete Eq. (5), as well as the values of W_{ix_i,jx_j} in Eq. (4) were calculated by solving the linearized Poisson-Boltzmann equation using the finite difference method.[52,53] A programme developed in our laboratory was used for the calculations. The following parameters were used in the calculations: CHARMM parameter set 22[54] partial atomic charges, including those of the titratable groups in protonated and deprotonated states; van der Waals radii taken from Rashin *et al.*[55]; solvent probe radius 1.4 Å; ion exclusion layer of 2 Å. Each snapshot structure was situated in a grid box (99 × 99 × 99) with grid spacing of 2.55 Å, which was gradually reduced using four consecutive focusing steps on each titratable group. The size of the focused boxes depends on the conformations of the titratable side chains in the different snapshot structures. On average, the final grid length was 0.24 Å. Solvent and protein relative dielectric constants were taken $\varepsilon_s = 78$ and $\varepsilon_p = 4$, respectively.

The pK calculations for denatured state were performed according the procedure described in our earlier articles.[41,44] A radius of 17.5 Å and dielectric constant of 25[44] were used for the low dielectric sphere representing the unfolded protein.

Coupling pK calculations with MD simulation

Protein conformers (snapshot structures) were collected each 5 ps during the last 7 ns of the MD simula-

tion. The calculations of electrostatic interactions were performed independently for each individual snapshot structure. The degree of deprotonation of the individual titratable sites, $\bar{\theta}_i$(pH), used in Eq. (2) (and then for calculation of ΔG^{el}) represent an arithmetic average of θ_i(pH) calculated for the individual snapshot structures. Test calculations showed that averaging over snapshot structures extracted in 5 ps and each 10 ps interval gives practically identical results. The results presented below are obtained by averaging over the interval of 10 ps.

RESULTS AND DISCUSSION

Starting from the X-ray structure we generated an ensemble of Lpp-56 conformers by a 10 ns MD simulation in explicit water. According to the usual criteria (C_α RMSD, radius of gyration, solute–solute and solute–solvent energy terms, intermolecular distances) the MD trajectory was well equilibrated in the last 7 ns of simulation, as to serve as a reliable model of the dynamic behavior of the protein. We first describe the results on prediction of the ionization properties of all Lpp-56 titratable groups. In a second part, we attempt quantification of the electrostatic contribution to Lpp-56 stability. Finally, we discuss a simple model providing clues about networked salt bridges as a possible player in the extremely slow unfolding transition of Lpp-56.

Ionisation equilibria

The calculated pK values of the titratable sites of Lpp-56 are listed in Table I. As already mentioned, we are not aware of any experimental data that could help assessing the reliability of this result. According to our experience with other proteins, for instance ribonuclease T_1,[56] we expect that the confidence interval of calculated pK values is about 0.5 pH units. Inspecting Table I one can notice that groups situated at equivalent positions along the sequence of the three peptide chains have different pK values, which can deviate from each other by as much as 3 pH units. This reflects the fact that the corresponding side chains within the three helices visit different sets of conformations, thus creating different time-averaged environment of the titratable sites. In contrast, due to the threefold noncrystallographic symmetry, the pK calculated for equivalent sites using the X-ray structure vary within the confidence interval. Hence, the large pK deviation is not due to the computational method. Furthermore, about half of the titratable sites display pK values that undergo larger shifts from their standard (pK_{mod}) values when the calculations are done by averaging over the snapshot structures, in comparison to pK shifts calculated with the X-ray structure (Table II). The extremely up-shifted pK of basic groups and extremely down-shifted pK of acidic groups reflect a strong favorable electrostatic influence of the environment, such as participation in salt bridges. For a MD-generated ensemble of structures, the magnitude of the pK shift of groups participating in salt bridge depends on the population of conformers bearing the particular salt bridge. The effect of reduction of the pK shift because of the temporary disruption of a salt bridge which is illustrated in Figure 2 on the example of the salt bridge formed between the C-terminal carboxyl group (chain C) and LysB54. (Hereafter, the polypeptide chain to which a particular residue belongs is indicated by a capital letter inserted between the side-chain name and the sequence number.) In the time window in which no salt bridge is formed, the average pK of the C-terminal carboxyl group of chain C is practically equal to pK_{mod}. A shift of the pK value of more than 6 pH units occurs if the salt bridge with LysB54 is formed. Considering the first 2.5 ns of the simulation, the calculated average pK is approximately in the middle between the values corresponding to free and salt bridged C-terminal carboxyl group, reflecting the fact that the fractional populations of the free and salt-bridged C-terminal carboxylate are also approximately equal. For the rest of the simulation after 2.5 ns, however, the population of the salt bridge is virtually 100% (that is, it does not break), and consequently, the average pK of the monitored C-terminal carboxyl group continuously reduces. The groups with extreme pK shifts, such as the aspartic acids at position 26 or the considered above C-terminal groups, participate in salt bridges which seldom disrupt during the MD simulation.

Short lifetime (between 300 and 500 ps) of salt bridges suggested by some previous MD simulations[31,57] cannot

Table II
Comparison of the pK Values of the Titratable Groups of Lpp-56 (I = 0.12) Calculated on the Basis of the X-ray Structure ($pK_{X\text{-}ray}$), Averaged Over the Structures Collected by MD Simulation (pK_{MD}) and of Unfolded State of the Protein (pK_U)

Group	p$K_{X\text{-}ray}$	pK_{MD}	pK_U
N-term	9.5	7.8	8.6
Asp07	1.6	2.2	3.6
Asp12	5.3	3.5	3.7
Asp21	2.2	3.3	3.6
Asp26	2.2	−3.4	3.7
Asp33	3.6	1.4	3.8
Asp39	3.4	2.1	3.6
Asp40	0.8	2.7	3.6
Asp49	1.2	2.0	3.5
Tyr55	13.3	16.0	9.5
Lys05	10.1	10.2	10.8
Lys19	11.0	10.5	10.9
Lys38	8.8	13.4	10.9
Lys54	10.4	13.0	10.8
Arg31	12.2	15.6	12.7
Arg43	13.7	13.8	12.7
Arg47	16.1	14.8	12.7
Arg56	113.0	12.5	12.6
C-term	3.8	−3.2	2.9

DOI 10.1002/prot

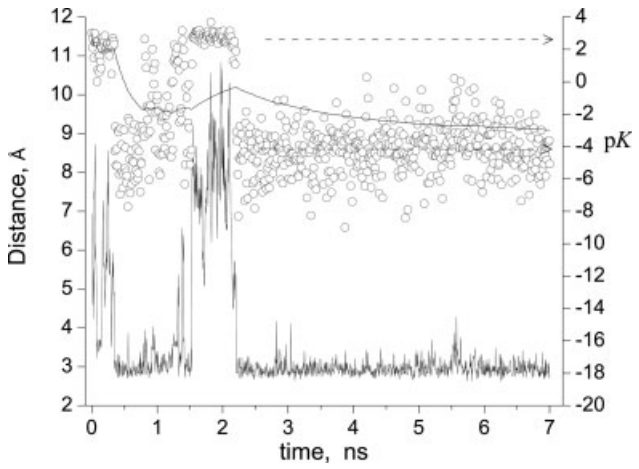

Figure 2

Salt bridge formation between the C-terminal carboxyl group (chain C) and Lys54 (chain B). Left ordinate: distances between the carboxyl oxygen atoms, (Oδ1+Oδ2)/2, and Nε of LysB54 (line). Right ordinate: snapshot pK values of the C-terminal carboxyl group (○), and time evolution of the average pK value of the C-terminal carboxyl group (line associated with the circles). The dashed arrows indicate the average pK when the carboxyl group does not form a salt bridge (upper arrow) and when salt bridge is formed (lower arrow).

be considered as a general rule. Salt bridges with lifetimes between 1 and 200 ns have been reported.[58–60] In principle, long lifetimes might be an artifact of the force field, if the oppositely charged atoms of the functional groups are trapped within short distances. To check this scenario, we performed MD simulation of the dimeric coiled-coil GCN4 using identical simulation protocol. This computational experiment revealed a different behavior of the titratable side chains involved in salt bridges: the lifetime of the salt bridges in GCN4 is essentially lower than that obtained for Lpp-56 (See Table IV). We conclude, therefore, that the long lifetime of some salt bridges and the extreme p*K* shifts calculated for Lpp-56 groups arise from the specific structural organization of the protein, rather than from a computational artifact.

The p*K* values calculated for the unfolded state of Lpp-56 are listed in Table II. All of them are non-negligibly shifted from their standard values. The average shift towards pK_{mod} of aspartic acids is 0.4 pH units, which is in accord with the experimental observation for other proteins.[61,62] This result reiterates the arising consensus that the denatured state is not an electrostatic "dummy" and that residual electrostatic effects in that state might contribute to the energetic balance stabilizing proteins.[63,64]

Electrostatic stabilization of Lpp-56

The electrostatic terms of the free energy calculated on the basis of the MD snapshot structures, ΔG^{el}_{MD}, and using the X-ray structure only, ΔG^{el}_{X}, are compared in Figure 3. The stabilizing contribution of the electrostatic interactions is substantially larger when calculated with the snapshot structures. This is an illustration of the effect of the reduced p*K* shifts calculated on the basis of the X-ray structure (Table II). The absolute values of ΔG^{el} have a meaning only in respect to the reference state, which here is an extreme low pH at which the folded and the unfolded states of the protein are identically protonated. Other values of ΔG^{el} will be obtained, as seen in Figure 3, if we choose the corresponding extreme alkaline pH. Therefore, no experimental verification of the absolute values of ΔG^{el} presented in Figure 3 can be made. However, if we assume that only electrostatic interactions change upon the change of pH, the relative pH dependence of ΔG^{el} can be verified experimentally. The unfolding free energy of Lpp-56 at pH 3 and pH 7 has been reported by Dragan *et al.*[5] From their data, $\Delta\Delta G^{therm}(\text{pH } 3 \rightarrow \text{pH } 7) = \Delta G^{therm}(\text{pH } 7) - \Delta G^{therm}(\text{pH } 3)$ is ~60 kJ mol^{-1}. This value is close to $\Delta\Delta G^{el}_{MD}$ (pH 3 → pH 7) = 63 kJ mol^{-1} obtained by us using MD snapshot structures averaging. In contrast, calculations done with the X-ray structure predict a much smaller free energy change between pH 3 and pH 7: $\Delta\Delta G^{el}_{X}$ (pH 3 → pH 7) = 29 kJ mol^{-1}. The presented results are clear evidence that the introduction of conformational flexibility in the calculations of electrostatic interactions in protein improves the predictive power of the computations.

From equilibrium and kinetic data collected in the presence of GdmCl as the denaturant we recently estimated the stability of Lpp-56 as $\Delta G^{Gdm} = 79 \pm 10$ kJ mol^{-1} pH 7.[4] At the same conditions, thermal unfolding experiments have predicted much higher stability,

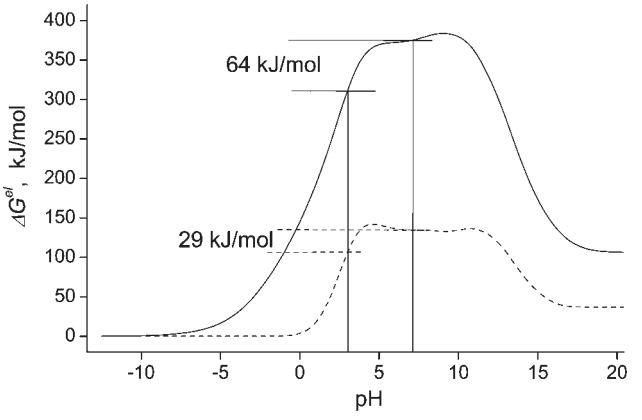

Figure 3

The electrostatic free energy as a function of pH calculated on the basis of MD simulation (continuous line) and the X-ray structure (dashed line).

$\Delta G^{\text{therm}} = 137$ kJ mol^{-1}.[5] It is commonly appreciated that GdmCl screens charge–charge interactions, so that the electrostatic contribution, ΔG^{el}, to ΔG^{Gdm} becomes smaller as the GdmCl concentration increases. Hence, the difference between ΔG^{Gdm} and ΔG^{therm} should be essentially electrostatic in nature.[6] ($\Delta G^{\text{Gdm}} < \Delta G^{\text{therm}}$ indicate that electrostatic effects are stabilizing the protein.) Taking into account the large, experimentally observed difference between ΔG^{Gdm} and ΔG^{therm} one can presume that the contribution of electrostatic interactions to the stability of the Lpp-56 is much larger than that observed for other proteins (typically less than 20 kJ mol^{-1}). Indeed, we have reasoned[4] that the linear extrapolation of the unfolding free energy from high GdmCl to zero denaturant to obtain ΔG^{Gdm} is very unlikely to underestimate the genuine stability of Lpp-56 by more than 20 kJ mol^{-1}. Nonetheless, the reasons for the large discrepancy between ΔG^{Gdm} and ΔG^{therm} remain obscure and, in fact, cannot be discerned by experiment. In the following, we discuss a computational approach to the problem.

It is believed that the energetic contribution of charge–charge interactions vanish around 1 *M* GdmCl. This statement, however, cannot be rigorously justified if one considers the influence of GdmCl of protein stability as a salt effect. The effect of ionic strength depends on the charge content[65,66] and on the charge configuration in the native state.[67] This suggests nonuniformed shielding of charge–charge interactions in folded and unfolded states.[68] Hence, the influence of salt concentration on stability is different for different proteins and no general statement about its magnitude can be done. We are interested in the influence of GdmCl on the magnitude of the electrostatic stabilization of Lpp-56. For concentrations of GdmCl less than 1*M* the reduction (or strengthening) of electrostatic stabilization can be considered as an effect of the ionic strength. In this way, the screening effect of GdmCl is reduced to calculations of ΔG^{el} for different ionic strengths:

$$\Delta^{\text{S}}\Delta G^{\text{el}} = \Delta G^{\text{el,S}} - \Delta G^{\text{el}} \qquad (6)$$

Superscript S indicates high salt concentration, $I = 1M$. The calculated pH dependence of $\Delta^{\text{S}}\Delta G^{\text{el}}$ is shown in Figure 4. Because ΔG^{el} and $\Delta G^{\text{el,S}}$ are defined up to additive constants, their values at the reference state (chosen to be at an extremely acidic pH) are set to zero and $\Delta^{\text{S}}\Delta G^{\text{el}}_{\text{ref}} = 0$. In respect to this reference state at pH 7 $\Delta^{\text{S}}\Delta G^{\text{el}} = -14$ kJ mol^{-1}. However, the latter figure has no sound physical meaning (and for that matter can not be considered as representing the difference $\Delta G^{\text{therm}} - \Delta G^{\text{Gdm}}$) since the reference states in low and high ionic strengths are equalized.

The difference between the reference states used to calculate ΔG^{el} and $\Delta G^{\text{el,S}}$ can be evaluated. For this purpose, we make use of the thermodynamic cycle

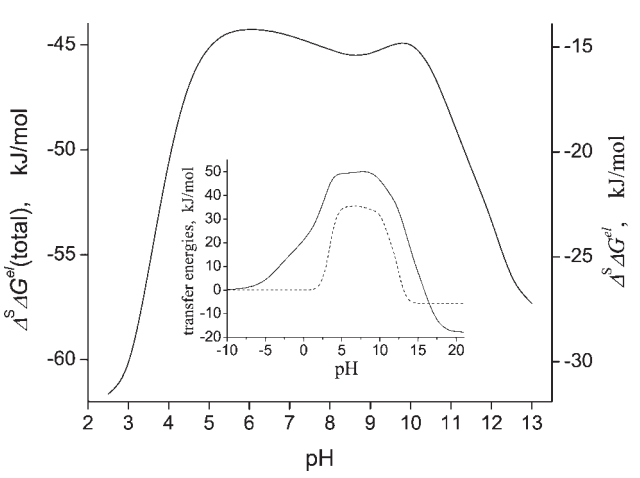

Figure 4

pH-Dependence of $\Delta^S\Delta G^{el}$ (right ordinate) and $\Delta^S\Delta G^{el}(pH)+\Delta G^{el}(F\rightarrow F^S)_{ref}$ (left ordinate). Insert: pH dependence of $\Delta G^{el}(F\rightarrow F^S)$ (continuous line) and $\Delta G^{el}(U\rightarrow U^S)$ (dashed line). The difference between these energies [Eq. (8)] gives $\Delta^S\Delta G^{el}$ (right ordinate).

$$\begin{array}{ccc} & \text{F} \xrightarrow{\Delta G^{\text{el}}} & \text{U} \\ \Delta G^{\text{el}}\ (\text{F} \rightarrow \text{F}^{\text{S}}) & \downarrow & \downarrow \quad \Delta G^{\text{el}}\ (\text{U} \rightarrow \text{U}^{\text{S}}) \\ & \text{F}^{\text{S}} \xrightarrow{\Delta G^{\text{el,S}}} & \text{U}^{\text{S}} \end{array}$$

The upper and lower horizontal limbs of the cycle represent unfolding at low ($I = 0.12M$) and high ($I = 1M$) ionic strengths, respectively. The left and right vertical limbs describe the hypothetical transfer of the folded (F) and unfolded (U) states, respectively, from low to high ionic strength conditions. According to the above thermodynamic cycle, the change of the electrostatic free energy of unfolding upon increase of the ionic strength given in Eq. (6) can also be expressed as:

$$\Delta^{\text{S}}\Delta G^{\text{el}} = \Delta G^{\text{el}}(\text{U} \rightarrow \text{U}^{\text{S}}) - \Delta G^{\text{el}}(\text{F} \rightarrow \text{F}^{\text{S}}). \qquad (7)$$

Consider the reference state. It is chosen such that all titratable sites are protonated, that is, the protein contains positive charges only. According to our model of the unfolded state the charges tend to adopt positions, at which the repulsive forces, and hence electrostatic interactions, are minimized. In this aspect the model mimics well the real situation, where the denatured state is flexible and the charges could rearrange as to minimize the energetic penalty of charge–charge repulsion. Therefore, in a first approximation, we can assume that for the reference state $\Delta G^{\text{el}}(\text{U} \rightarrow \text{U}^{\text{S}})_{\text{ref}}$ is small and can be neglected. At pH far from the reference state $\Delta G^{\text{el}}(\text{U} \rightarrow \text{U}^{\text{S}})$ cannot be neglected, as illustrated in the insert of Figure 4. Analogous assumption for the reference state of the folded protein is not valid. The positions of the charges

DOI 10.1002/prot

are fixed by the three-dimensional structure of the molecule, so that unfavorable electrostatic interactions between positive charges are sizeable in the reference state. Formally, the charge–charge interactions in the reference state can be calculated by Eq. (4) where the sequence $\mathbf{x} = (0, \ldots, 0)$ corresponds to all titratable sites in their protonated forms. The change of the charge–charge interactions upon the transfer of the native form of the protein in the reference state from low to high ionic strength calculated in this way amounts to -30 kJ mol^{-1} (the reference state is stabilized at high ionic strength because of the reduction of the repulsive interactions). Thus, the total change of the electrostatic free energy caused by the screening effect of GdmCl calculated for pH 7 becomes $\Delta^S\Delta G^{el}(\text{total}) = -45$ kJ mol^{-1}.

A certain underestimation of the value of $\Delta^S\Delta G^{el}(\text{total})$ is to be expected because the calculations at high ionic strength were preformed with the linearised Poisson-Boltzmann equation. The linearized and the nonlinear Poisson-Boltzmann equations give very similar results at least up to $I = 0.5M$, underestimating the reduction of electrostatic energy because of the salt effect by about 10%.[69] Even ignoring this underestimation, it is clear that the value of $\Delta^S\Delta G^{el}(\text{total})$ represents a significant energetic contribution. The estimated 45 kJ mol^{-1} unfolding free energy reduction stemming from charge screening by salt (GdmCl for that matter) exceeds our previous estimate (10–20 kJ mol^{-1}). Rather, it approaches the value (~60 kJ mol^{-1}) corresponding to the difference between ΔG^{Gdm} measured by us[70] and ΔG^{therm} obtained by Dragan *et al.*[5]

We would like to add a note of caution in interpreting the numerical value of the charge–charge contribution to the stability of Lpp-56, presumed to represent the total difference of experimentally measured unfolding free energies ($\Delta G^{therm} - \Delta G^{Gdm}$). It has been argued that both, the native and unfolded states are not fixed in their properties, depending on the physical agent used to shift the equilibrium between these states.[9] The calculations presented in this work consider only the ionic strength effect. The influence of the electrolyte type, including protein–ion binding effects, is ignored. This is in fact ignoring any denaturant-specific differences in the structure of the folded and the unfolded states. In spite of all these considerations, we conclude that indeed the difference between the unfolding free energies of Lpp-56 measured by the two different experimental approaches is to a large extent due to the screening effect of GdmCl.

Role of the salt bridges in unfolding kinetic of Lpp-56

Although folding of Lpp-56 is also slow, it appears that the high thermodynamic stability originates from an extremely low unfolding rate. On the basis of the strong dependence of the unfolding rate constant on the concentration of salt (GdmCl) we have speculated that there is a significant electrostatic component to the activation energy barrier for unfolding. Here, we ask whether the known high kinetic stability of Lpp-56 can be related to this electrostatic component, in particular to the presence of salt bridges which seldom or never disrupt during the MD simulation.

We have mentioned that the trimeric superhelix is clamped along its length by rings of interhelical salt bridges (see Fig. 1). Since the prevailing majority of them have long lifetimes it is worth having a closer look at their behavior. In the course of the MD simulation we observe formation of 15 salt bridges. Among them 12 are interhelical links forming the charge rings illustrated in Figure 1. The organization of rings and the lifetimes of the salt bridges constituting them are specified in Table III. In the following we consider a salt bridge being

Table III
Interhelical Salt Bridges in Lpp-56

Ring 1	*p*
Asp21A—Lys19C	0.02
Asp21B—Lys19A	0.01
Asp21C—Lys19B	0
Ring 2	***p***
ArgA31—AspC26	1
ArgB31—AspA26	0.98
ArgC31—AspB26	0.99
Ring 3-cluster	***p***
AspA33 — LysB38 ArgA43 — AspA40 AspA39	0.9
AspB33 LysC38 ArgB43 — AspB40 AspB39	0.79
AspC33 ArgC43 — AspC40 — LysA38 AspC39	0.95
Ring 4	***p***
AspA49—ArgC47	0.52
AspB49—ArgA47	0.35
AspC49—ArgB47	0.92
Ring 5	***p***
CtrA56—LysC54	0.95
CtrB56—LysA54	0.89
CtrC56—LysB54	0.85
Ring 6	***p***
CtrA56—TyrC55	0.99
CtrB56—TyrA55	0.99
CtrC56—TyrB55	0.99

The parameter *p* is the ratio between the lifetime of a salt bridge and the total time (7 ns) of the MD simulation used to collect snapshot structures.

formed if at least one donor-acceptor distance between the bridged groups to be less than 3.1 Å. This distance corresponds to the upper limit for a stable hydrogen bond. Although electrostatic attraction between the interacting groups is significant even at distances larger than the chosen criterion such configurations lose the features of a hydrogen bond.

The group of salt bridges close to the N-terminus (top in Fig. 1) does not form a ring of interhelical rings. Of certain interest are the salt bridges forming ring 1. In the X-ray structure all these salt bridges are well defined, with proton donor-to-proton acceptor distances between 2.6 and 2.9 Å, corresponding to an ideal hydrogen bond. However, it turned out that the lifetime of these salt bridges is negligible during the MD simulation. Almost opposite is the situation in Ring 2, where the salt bridges practically do not disrupt during the MD simulation, whereas in the X-ray structure only one of them satisfies the above criterion. The difference in the behavior of these salt bridges is reflected by the large difference in the pK values of participating groups (see Table II for comparison).

Ring 3 is a cluster of salt bridges involving also intrahelical links. The pairs within the cluster exchange their partners as indicated in Table III. This feature is also illustrated in Figure 5 for the case of LysC38. This residue adopts conformations at which it preferably interacts with AspB33 or with AspB40. The lifetime of the salt bridges this side chain forms is plotted in Figure 6. It is important for our further considerations to note that the cross-link between the helices B and C is intact in spite of the mobility of the lysine side chain. Similar behavior is also observed for the intramolecular salt bridges with the participation of Arg43 (see Table III). This observation leads us to the conclusion that the stabilization role of this ring is achieved by both, favorable interhelical electrostatic interactions and reduction of entropic losses.

Ring 4 displays properties similar to those of Rings 2 and 5, yet it appears more "loose" judging from the average lifetime of the participating salt bridges (Table III).

Ring 5 is also stabilized by a network involving the hydrogen bond between C-terminal carboxyl groups and the hydroxyl groups of Tyr55. In contrast to the network of Ring 3, here the configurations HOη(TyrY55)–(LysX56)COO^{-}–NζH_3^+(LysX56) remain stable with lifetime of at least 85% (see Table III). As illustrated in Figure 7, the hydrogen bonds (Lys56)$COO^{-}\cdots$HOη(Tyr55) are interhelical and are expected to contribute to the stabilization of the bundle in this region. Because of this, we consider these hydrogen bonds formally as a separate ring (Ring 6).

The overview of the rings of interhelical salt bridges suggests that they should play an important role in the stabilization of the native three-dimensional structure of Lpp-56. On the basis of this, we hypothesize that the long life time of the prevailing majority of interhelical salt bridges contributes for structural stability of Lpp-56 as well as for its low unfolding rate.

Assume for simplicity that the protein unfolding is initiated by the disruption of the salt bridge rings. We consider a ring as broken if at least two interhelical salt bridges within this ring are simultaneously disrupted. This assumption reflects the properties of quasi-symmetric, noncovalent homotrimers, where dissociation of one monomer requires simultaneous disruption of two sets of quasi-symmetric interactions.[71] Two salt bridges being disrupted, one of the helices in the region of a given ring could more easily move away from the other two. The hydrophobic packing is weaken (leading to enthalpic destabilization), the mobility of groups increases (making the molecule more sensitive to thermal fluctuations), the hydrophobic core becomes partially hydrated. These effects promote non-native conformations. Such conformations may be stabilized and may propagate if the neighboring ring is broken, otherwise the native conformation is stabilized. Since unfolding is coupled to chain dissociation, according to this scenario, a successful attempt for unfolding occurs if all salt bridge rings break simultaneously. The probability a ring, i, to be disrupted can be calculated by

$$p_i = \overline{p_{AC}}p_{BA}p_{CB} + p_{AC}\overline{p_{BA}}p_{CB} + \overline{p_{AC}}p_{BA}\overline{p_{CB}} + \overline{p_{AC}}p_{BA}p_{CB}, \quad (8)$$

where p_{XY} is the probability a cross-link (an interhelical salt bridge) between helix X and helix Y to exist. The probability p_{XY} is the parameter p (given in Table III) calculated as the ratio between the lifetime of a salt bridge connecting helices X and Y and the total time of simulation. The probability a cross-link between helix X and helix Y to be disrupted is then $\overline{p_{XY}} = 1 - p_{XY}$. Equation (8) comprises of the sum of the probability all salt bridges in a ring to be disrupted (the first term on its right hand side) and the probabilities one salt bridge (p_{AC} or p_{BA} or p_{CB}) to be intact while the other two are disrupted. The equation is valid if the events XY are independent. Since we have not found any correlation between the breaking and formation of the salt bridges within the rings, the above condition can be considered as fulfilled. The probability of all rings are to be disrupted simultaneously, that is, the probability of a successful attempt for unfolding, is then

$$p_{\mathrm{unf}} = \prod_{i=1}^{6} p_i = 2.0 \times 10^{-11}.$$

One can consider the process of unfolding as a series of events (independent or related), which stabilize non-native conformations. The unfolding rate will be then limited by the events with lower probability. In this context, we relate the extremely low value of the probability p_{unf} with the

DOI 10.1002/prot

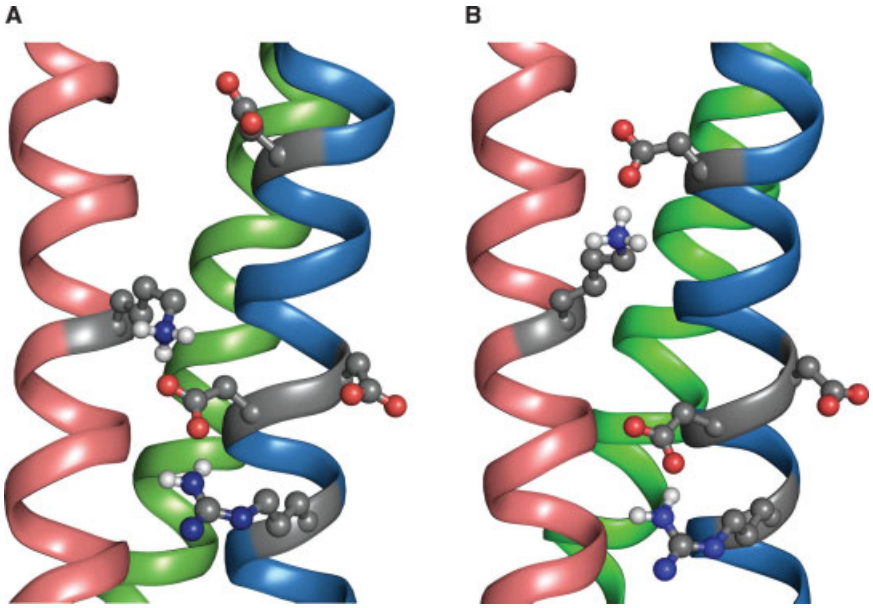

Figure 5

Part of the salt bridge network in Ring 3 (Table III). Snapshot structures ***A****: Salt bridge AspB33-LysC38. Snapshots structure* ***B****: Salt bridge AspB40-LysC38. Image reproduced using The PyMOL Executable Build, (2005) DeLano Scientific LLC, Sauth San Francisco, CA, USA.*

likewise low unfolding rate constant measured for Lpp-56. This correlation is valid if the time interval of the MD simulation is long enough to ensure ergodicity of the system. An evidence for this is in good agreement between the calculated change of the electrostatic free energy with pH, $\Delta\Delta G^{el}_{MD}$ (pH 3 → pH 7), and the experimentally observed $\Delta\Delta G^{therm}$(pH 3 → pH 7). An additional indirect evidence is the value of p_{unf} calculated for the GCN4 leucine zipper. This protein has a spatial organization similar to that of Lpp-56, although it consists of two, instead of three α-helices. The lifetimes of the interhelical salt

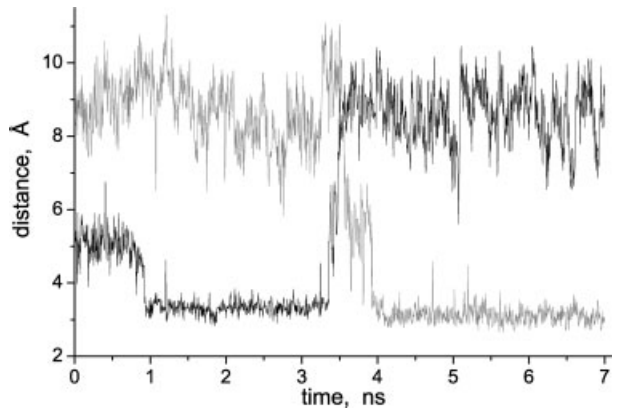

Figure 6

Lifetime of salt bridges AspB33-LysC38 (grey line) and AspB40-LysC38 (black line), The distance plotted is between the average coordinates of the carboxyl oxygen atoms, (Oδ1+Oδ2)/2, of the aspartic acid and the Nζ atom of LysC38.

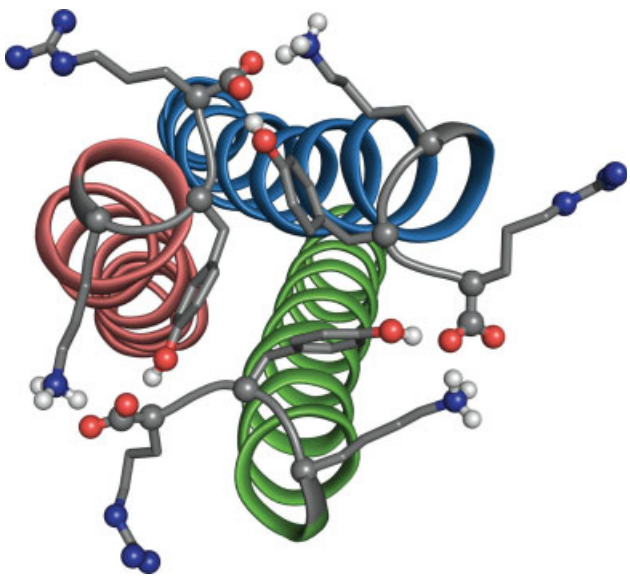

Figure 7

C-terminal Rings 5 and 6. Image reproduced using The PyMOL Executable Build, (2005) DeLano Scientific LLC, Sauth San Francisco, CA, USA.

Table IV
Interhelical Salt Bridges in GCN4 Leucine Zipper

Ring 1	*p*
LysA15—GluB20	0.48
LysB15—GluA20	0.30
Ring 2	***p***
GluA22—LysB27	0.12
GluB22—LysA27	0.45
Ring 3	***p***
ArgA25—CtrB31	0.07
ArgB25—CtrA31	0.10

The parameter *p* is described in the legend of Table III.

bridges in GCN4, grouped in rings by analogy with Lpp-56, are listed in Table IV. To maintain the assumptions as close as possible to those made for Lpp-56, a ring is considered as disrupted, if it consists of only one interhelical salt bridge. The probability of such an event is then

$$p_i = 1 - p_{AB}p_{BA}$$

and $p_{\mathrm{unf}} = \Pi p_i = 0.79$. The probabilities p_{AB} and p_{BA} correspond to symmetric salt bridges connecting the two helices of GCN4. However the probabilities are different (Table IV) because of the independent side chains movement of the two helices. If we assume that a ring breaks when both salt bridges are disrupted

$$p_i = \overline{p_{AB}p_{BA}}$$

and $p_{\mathrm{unf}} = 0.12$. The values of p_{unf} calculated for GCN4 are essentially larger than that calculated for Lpp-56. If we relate the probabilities for successful unfolding of the two proteins with their unfolding rate constants, it follows from the $p_{\mathrm{unf}}^{\mathrm{GCN4}}/p_{\mathrm{unf}}^{\mathrm{Lpp}}$ ratio that GCN4 unfolds 3.9×10^{10} to 5.9×10^{9} faster than Lpp-56. Unfortunately, a direct comparison with the actual unfolding constants is not possible, since the unfolding constant of Lpp-56 is not precisely known. However, it is $>1 \times 10^{-11}$ s^{-1}. Since the unfolding rate constant of GCN4 is $\sim 2 \times 10^{-2}$ s^{-1},[72] the ratio of the experimentally measured rate constants is $k_{\mathrm{unf}}^{\mathrm{GCN4}}/k_{\mathrm{unf}}^{\mathrm{Lpp}} > 2 \times 10^{9}$. On the basis of the good agreement between our prediction and experiment observation, we conclude that the enormously low unfolding rate of Lpp-56 is essentially related to electrostatic interactions, and in particular, to the stability of the salt bridges.

It appears that the simple assumption underlying the model capture important features of Lpp-56 (and probably other coiled coils). The careful thermodynamic analysis of Dragan *et al.*[5] led the authors describe the Lpp-56 unfolding transition state as native-like, that is "... the helices forming this coiled coil are still not sufficiently separated ... yet at this stage extensive disruption of some short-range enthalpic interactions takes place. ..." Furthermore, they analyze the activation enthalpy and entropy of unfolding and conclude: "It appears thus that unfolding of the rigid three-stranded coiled coil starts from the simultaneous disruption of all van der Waals contacts between the strands, and since the probability of that is low, the process is slow." Such a picture is fully complementary to the basic assumptions of the presented model. It appears that the long-living salt bridges, which are staggered along the rod-like molecule, effectively prevent propagation of local unfolding events. Since it is believed that end-fraying is a factor destabilizing coiled coils, of special interest is the fact that the C-terminus of the molecule is tightly constrained through electrostatic interactions within Rings 5 and 6.

Finally, we would like to add that also in other proteins salt bridges which cross-link secondary structure elements, or are present at the interface of sub-units might provide a source of kinetic stabilization, possibly by reducing the activation entropy for unfolding, thus increasing the activation energy for unfolding.[60,73–75] It should be noted, however, that the stabilizing effect of the salt bridge charge–charge interactions is a consequence of the dynamic properties of the groups involved. These properties are, on the other hand, determined by the dynamic properties of the environment, which may or may not tolerate conformational freedom of the charged side chains, in this way regulating the salt bridge lifetime. In general, this feature cannot be recognized from a single, say crystal, protein structure. In this context, the combination of MD-based analysis and p*K* calculations might serve as a useful guide for experimentalists in mutation-based approaches.

ACKNOWLEDGMENTS

The molecular dynamics simulations were performed on the Matterhorn Beowulf cluster at the Informatikdienste of the University of Zurich. The authors thank C. Bollinger, Dr. T. Steenbock, and Dr. A. Godknecht for setting up and maintaining the cluster.

REFERENCES

1. Lupas AN, Gruber M. The structure of α-helical coiled coils. Adv Protein Chem 2005;70:37–78.
2. Shu W, Liu J, Ji H, Lu M. Core structure of the outer membrane lipoprotein from *Escherichia coli* at 1.9 Å resolution. J Mol Biol 2000;299:1101–1112.
3. DiRienzo JM, Nakamura K, Inouye M. The outer membrane proteins of gram-negative bacteria: biosynthesis, assembly, and functions. Annu Rev Biochem 1978;47:481–532.
4. Bjelic S, Karshikoff A, Jelesarov I. Stability and folding/unfolding kinetics of the homotrimeric coiled coil Lpp-56. Biochemistry 2006; 45:8931–8939.
5. Dragan AI, Potekhin SA, Sivolob A, Lu M, Privalov PL. Kinetics and thermodynamics of the unfolding and refolding of the three-stranded a-helical coiled coil, Lpp-56. Biochemistry 2004;43:14891–14900.
6. Ibarra-Molero B, Loladze VV, Makhatadze GI, Sanchez-Ruiz JM. Thermal versus guanidine-induced unfolding of ubiquitin. An analysis in terms of the contributions from charge-charge to interactions protein stability. Biochemistry 1999;38:8138–8149.

DOI 10.1002/prot

7. Makhatadze GI. Thermodynamics of protein interactions with urea and guanidinium hydrochloride. J Phys Chem B 1999;103:4781–4785.
8. Ibarra-Molero B, Sanchez-Ruiz JM. A model-independent, nonlinear extrapolation procedure for the characterization of protein folding energetics from solvent-denaturation data. Biochemistry 1996;35:14689–14702.
9. Ferreon AC, Bolen DW. Thermodynamics of denaturant-induced unfolding of a protein that exhibits variable two-state denaturation. Biochemistry 2004;43:13357–13369.
10. Pfeil W. Protein stability and folding: a collection of thermodynamic data. New York: Springer-Verlag; 2001.
11. Monera OD, Kay CM, Hodges RS. Protein denaturation with guanidine-hydrochloride or urea provides a different estimate of stability depending on the contributions of electrostatic interactions. Protein Sci 1994;3:1984–1991.
12. Humphrey W, Dalke A, Schulten K. VMD: visual molecular dynamics. J Mol Graph 1996;14:33–38.
13. Yang A-S, Honig B. On the pH dependence of protein stability. J Mol Biol 1993;231:459–474.
14. Langella E, Improta R, Crescenzi O, Barone V. Assessing the acid-base and conformational properties of histidine residues in human prion protein (125–228) by means of pK_a calculations and molecular dynamics simulations. Proteins 2006;64:167–177.
15. Bashford D, Karplus M. Multiple-site titration curves of proteins: an analysis of exact and approximate methods for their calculation. J Phys Chem 1991;95:9556–9561.
16. Bashford D, Karplus M. pK_a's of ionizable groups in proteins: atomic detail from a continuum electrostatic model. Biochemistry 1990;29:10219–10225.
17. Matthew JB. Electrostatic effects in proteins. Annu Rev Biophys Biomol Struct 1985;14:387–417.
18. Weast RC, editor. Dissociation constants of organic bases in aqueous solution. Handbook of chemistry and physics, 51st edition. Ohio: The Chemical Rubber CO.; 1971. p D117.
19. Yang A-S, Gunner MR, Sampogna R, Sharp K, Honig B. On the calculation of pK_as in proteins. Proteins 1993;15:252–265.
20. You TJ, Bashford D. Conformation and hydrogen ion titration of proteins: a continuum electrostatic model with conformational flexibility. Biophys J 1995;69:1721–1733.
21. Beroza P, Case DA. Including side chain flexibility in continuum electrosttatic calculations of protein titration. J Phys Chem 1996;100:20156–20163.
22. Alexov E, Gunner MR. Incorporating protein conformational flexibility into the calculation of pH-dependent protein properties. Biophys J 1997;72:2075–2093.
23. Alexov EG, Gunner MR. Calculated protein and protonmotion coupled to electron transfer: electron transfer from Q_A-Q_B to Q_B in bacterial photosynthetic reaction centers. Biochemistry 1999;38: 8253–8270.
24. Georgescu RE, Alexov E, Gunner MR. Combining conformational flexibility and continuum electrostatics for calculating pK_as in proteins. Biophys J 2002;83:1731–1748.
25. Koumanov A, Benach J, Atrian S, Gonzàlez-Duarte R, Karshikoff A, Ladenstein R. The catalytic mechanism of Drosophila alcohol dehydrogenase: evidence for a proton relay modulated by the coupled ionization of the active site lysine/tyrosine pair and a NAD^+ ribose OH switch. Proteins 2003;51:289–298.
26. Bashford D, Gerwert K. Electrostatic calculations of the pK_a values of ionizable groups in bacteriorhodopsin. J Mol Biol 1992;224:473–486.
27. Yang A-S, Honig B. Structural origin of pH and ionic strength effects on protein stability. Acid denaturation of sperm whale apomyoglobin. J Mol Biol 1994;237:602–614.
28. Zhou H-X, Vijayakumar M. Modeling of protein conformational fluctuations in pK_a prediction. J Mol Biol 1997;267:1002–1011.
29. van Vlijmen HWT, Schaefer M, Karplus M. Improving the accuracy of protein pK_a calculations—conformational averaging versus the average structure. Proteins 1998;33:145–158.
30. Baptista AM, Teixeira VH, Soares CM. Constant-pH molecular dynamics using stochastic titration. J Chem Phys 2002;117:4184–4200.
31. Koumanov A, Karshikoff A, Friis EP, Borchert TV. Conformational averaging in pK calculations. Improvement and limitations in prediction of ionization properties of proteins. J Phys Chem B 2001;105:9339–9344.
32. Pace CN, Alston RW, Shaw KL. Charge-charge interactions influence the denatured state ensemble and contribute to protein stability. Protein Sci 2000;9:1395–1398.
33. Schaefer M, Sommer M, Karplus M. pH-dependence of protein stability: absolute electrostatic free energy difference between conformations. J Phys Chem B 1997;101:1663–1683.
34. Warwicker J. Simplified methods for pK(a) and acid pH-dependent stability estimation in proteins: removing dielectric and counterion boundaries. Protein Sci 1999;8:418–425.
35. Phelan P, Gorfe AA, Jelesarov I, Marti DN, Warwicker J, Bosshard HR. Salt bridges destabilize a leucine zipper designed for maximized ion pairing between helices. Biochemistry 2002;41:2998–3008.
36. Elcock AH. Realistic modeling of the denatured states of proteins allows accurate calculations of the pH dependence of protein stability. J Mol Biol 1999;294:1051–1062.
37. Zhou HX. A Gaussian-chain model for treating residual charge-charge interactions in the unfolded state of proteins. Proc Natl Acad Sci USA 2002;99:3569–3574.
38. Zhou HX. Residual electrostatic effects in the unfolded state of the N-terminal domain of L9 can be attributed to nonspecific nonlocal charge-charge interactions. Biochemistry 2002;41:6533–6538.
39. Zhou HX. Dimensions of denatured protein chains from hydrodynamic data. J Phys Chem B 2002;106:5769–5775.
40. Zhou HX. Direct test of the gaussioan-chain model for treating residual charge-charge interactions in the unfolded state of proteins. J Am Chem Soc 2003;125:2060–2061.
41. Kundrotas PJ, Karshikoff A. Model for calculations of electrostatic interactions in unfolded proteins. Phys Rev E 2002;65(1 Part 1): 011901.
42. Kundrotas PJ, Karshikoff A. Effects of electrostatic interactions on dimensions of unfolded polypeptide chains with various charge distributions: monte carlo study. J Chem Phys 2003;119:3574–3581.
43. Kundrotas PJ, Karshikoff A. Charge sequence coding in statistical modeling of unfolded proteins. Biochim Biophys Acta 2004;1702:1–8.
44. Kundrotas PJ, Karshikoff A. Modeling of denatured state for calculations of electrostatic contribution to protein stability. Protein Sci 2002;11:1681–1686.
45. Lindahl E, Hess B, van der Spoel D. GROMACS 3.0: a package for molecular simulation and trajectory analysis. J Mol Model 2001; 7:306–317.
46. Jorgensen WL, Chandrasekhar J, Madura JD, Impey RW, Klein ML. Comparison of simple potential functions for simulating liquid water. J Chem Phys 1983;79:926–935.
47. Hess B, Bekker H, Berendsen HJC, Fraaije JGEM. LINCS: a linear constraint solver for molecular simulations. J Comput Chem 1997; 18:1463–1472.
48. Miyamoto S, Kollman PA. Settle–an analytical version of the shake and rattle algorithm for rigid water models. J Comput Chem 1992;13:952–962.
49. Darden T, York D, Pedersen L. Particle mesh ewald—an N.log(N) method for ewald sums in large systems. J Chem Phys 1993;98: 10089–10092.
50. Berendsen HJC, Postma JPM, Vangunsteren WF, Dinola A, Haak JR. Molecular-dynamics with coupling to an external bath. J Chem Phys 1984;81:3684–3690.
51. Karshikoff A. A simple algorithm for calculation of multiple site titration curves. Protein Eng 1995;8:243–248.
52. Warwicker J, Watson NC. Calculation of the electric field potential in the active site cleft due to α-helix dipoles. J Mol Biol 1982;157: 671–679.

53. Nicholls A, Honig B. A rapid finite difference algorithm, utilizing successive over-relaxation to solve the Poisson-Boltzmann equation. J Comput Chem 1991;12:435–445.
54. Brooks BR, Bruccoleri RE, Olafson BD, States DJ, Swaminathan S, Karplus M. CHARMM: a program for macromolecular energy, minimization, and dynamics calculations. J Comput Chem 1983; 4:187–217.
55. Rashin AA, Iofin M, Honig B. Internal cavities and buried waters in globular proteins. Biochemistry 1986;25:3619–3625.
56. Koumanov A, Spitzner N, Rüterjans H, Karshikoff A. Ionisation properties of titratable groups in ribonuclease T_1. II. Electrostatic analysis Eur Biophys J 2001;30:198–206.
57. Caflisch A, Karplus M. Acid and thermal denaturation of barnase investigated by molecular dynamics simulation. J Mol Biol 1995;252:627–708.
58. Gruia AD, Fischer S, Smith JC. Kinetics of breaking a salt-bridge critical in protein unfolding. Chem Phys Lett 2004;385:337–340.
59. Sheldahl C, Harvey SC. Molecular dynamics on a model for nascent high-density lipoprotein: role of salt bridges. Biophys J 1999;76: 1190–1198.
60. Huang XQ, Zhou HX. Similarity and difference in the unfolding of thermophilic and mesophilic cold shock proteins studied by molecular dynamics simulations. Biophys J 2006;91:2451–2463.
61. Tan Y-J, Oliveberg M, Davis B, Fersht AR. Perturbed pK_a-values in the denatured states of proteins. J Mol Biol 1995;254:980–992.
62. Tollinger M, Forman-Kay JD, Kay LE. Measurement of side-chain carboxyl pK_a values of glutamate and aspartate residues in an unfolded protein by multinuclear NMR spectroscopy. J Am Chem Soc 2002;124:5714–5717.
63. Whitten ST, Garcia-Moreno B. pH dependence of stability of staphylococcal nuclease: evidence of substantial electrostatic interactions in the denatured state. Biochemistry 2000;39:14292–14304.
64. Cho J-H, Raleigh DP. Mutational analysis demonstrates that specific electrostatic interactions can play a key role in the denatured state ensemble of proteins. J Mol Biol 2005;353:174–185.
65. Zhou H-X, Dong F. Electrostatic contributions to the stability of a thermophilic cold shock protein. Biophys J 2003;84:2216–2222.
66. Spencer DS, Xu K, Logan TM, Zhou HX. Effects of ph, salt, and macromolecular crowding on the stability of fk506-binding protein: an integrated experimental and theoretical study. J Mol Biol 2005; 351:219–232.
67. Lee KK, Fitch CA, Lecomte JTJ, García-Moreno BE. Electrostatic effects in highly charged proteins: salt sensitivity of pK_a values of histidines in staphylococcal. Biochemistry 2002;82: 5656–5667.
68. Lindman S, Xue WF, Szczepankiewicz O, Bauer MC, Nilsson H, Linse S. Salting the charged surface: pH and salt dependence of protein G B1 stability. Biophys J 2006;90:2911–2921.
69. Rocchia W, Alexov E, Honig B. Extending the applicability of the nonlinear Poisson-Boltzmann equation: multiple dielectric constants and multivalent ions. J Phys Chem 2001;105:6507–6514.
70. Karshikoff A, Ladenstein R. The role of electrostatic interactions in the stabilization of proteins from thermophiles. In: Uversky VN, Permyakov EA, editors. Protein structures: methods in protein structure and stability analysis. New York: Nova Science Publishers; 2006.
71. Forrer P, Chang C, Ott D, Wlodawer A, Plückthun A. Kinetic stability and crystal structure of the viral capsid protein SHP. J Mol Biol 2004;344:179–193.
72. Ibarra-Molero B, Makhatadze GI, Matthews CR. Mapping the energy surface for the folding reaction of the coiled-coil peptide GCN4-p1. Biochemistry 2001;40:719–731.
73. Cavagnero S, Debe DA, Zhou ZH, Adams MWW, Chan SI. Kinetic role of electrostatic interactions in the unfolding of hyperthermophilic and mesophilic rubredoxins. Biochemistry 1998;37:3369–3376.
74. Bellapadrona G, Chiaraluce R, Consalvi V, Ilari A, Stefanini S, Chiancone E. The mutations Lys 114 to Gln and Asp 126 to Asn disrupt an intersubunit salt bridge and convert *Listeria innocua* DPS into its natural mutant *Listeria monocytogenes* Dps. Effects on protein stability at low pH. Proteins 2007;66:975–983.
75. Zubillaga RA, Garcia-Hernandez E, Camarillo-Cadena M, Leon M, Polaina J. Effect of a new ionic pair on the unfolding activation barrier of β-glucosidase B. Protein Pept Lett 2006;13:113–118.

 DOI 10.1002/prot